Time resolved nanocrystallite growth of cerium oxide and lanthanum-doped cerium oxide using X-ray diffraction — unusually low nanocrystallite growth as a function of chemistry and drying method.

Brian Neltner,[†] Scott Speakman,[†] Dong Soo Yun,[†] and Angela Belcher[*,†,‡]

Department of Materials Science and Engineering, Massachusetts Institute of Technology, Cambridge MA, and Department of Biological Engineering, Massachusetts Institute of Technology, Cambridge MA

E-mail: belcher@mit.edu

Abstract

Ceria is an ceramic which acts as an excellent redox support in catalytic reactions, and is generally much more active when present as a nanocrystalline material than as a bulk crystal. In this work, the sintering of ceria nanocrystals both with and without lanthanum dopant was investigated as a function of initial size by using in-situ heat treatment combined with rapid x-ray diffraction pattern acquisition ($\sim$1 measurement per minute) of the {200} CeO_2 peak. Additionally, the oxygen vacancy concentration of the nanocrystals was estimated by using principle component analysis of x-ray photoelectron spectra and shown to be as high as 18%. Finally, by modifying the drying method and precursors used, we were able to investigate possible mechanisms preventing sintering in the material. Initial size was controlled between 1.3

[*]To whom correspondence should be addressed
[†]MIT Department of Materials Science and Engineering
[‡]MIT Department of Biological Engineering

and 7 nm by using varying amounts of hydrogen peroxide while hydrolysing cerium chloride with sodium hydroxide.

CeO_2 (ceria) is a ceramic with a great deal of promise as a co-catalyst with many noble metals such as rhodium, nickel, gold, and platinum in the production of hydrogen gas suitable for use in a fuel cell from ethanol and water.[1] For example, rhodium and nickel, when supported on ceria, resulted in ethanol conversion at only 375°C.[2,3] Additionally, ceria is used in many systems such as catalytic converters to improve efficiency and decrease the required loadings of expensive noble metals to achieve good performance.[4–6]

Ceria acts as an excellent redox support due to highly mobile oxygen atoms in the lattice.[6,7] By exchanging oxygen with the substrate, supported noble metals can easily change oxidation state, allowing for enhancement of their catalytic performance. For example, the binding of a gold atom to a {111} surface ceria oxygen vacancy results in a decreased binding energy to CO. The decreased binding energy allows gold to catalytically oxidize CO without becoming poisoned by permanent CO binding.[8,9]

It has been shown that ceria nanocrystals tend to have an increased oxygen vacancy concentration as their size is reduced due to a combination of an increased probability of surface defects, and a change in the lattice constant of the bulk material.[10,11] Ceria shows a substantial increase in catalytic efficiency as particle size decreases and surface area increases, most likely due to this increased availability of oxygen vacancies for the metal catalyst to bind to as well as increased oxygen diffusion rate inside the crystal.[2,12]

While very small nanocrystals of ceria are extremely promising in terms of catalytic activity, relatively little work has been reported investigating their thermal stability. Kuo et al investigated the bulk behavior of relatively large nanocrystals (14 nm and over).[13,14] Work has also been done investigating the change to sintering behavior caused by incorporating lanthanum as a dopant.[15,16] Other research has investigated the properties of loosely agglomerated CeO_2 powders, and found that high levels of hydrogen peroxide in the synthesis result in smaller crystallite sizes, more amorphous material, residual surface species such as η^2-peroxides and hydroxides, and more loosely ag-

glomerated final products.[16–20] However, none of the existing surveys investigate the time-resolved thermal properties or energetics of the extremely small, high catalytic activity nanocrystals which are most desirable for use in catalytic systems.

Results and discussion

Synthesis

Using a method derived from that developed by Yamashita *et al*,[21] nanocrystals were formed using precipitation via hydrolysis in aqueous solution of cerium chloride heptahydrate or cerium nitrate by adding NaOH with simultaneous oxidation using hydrogen peroxide. Nanocrystals of CeO_2 of varying sizes were formed by stirring 100 mL of 100 mM metal chloride solution in a 250mL Erlenmeyer flask for 30 minutes. Next, varying amounts of 30 wt% H_2O_2 were added to 100 mL of 300 mM NaOH solution in a separate flask with water added to a total volume of 150 mL. The mixed NaOH/H_2O_2 solution is added rapidly to the metal chloride solution. By varying the amount of hydrogen peroxide between a molar ratio of 0.0580:1 and 58:1, size was controlled between 1.3 and 7 nm.

In typical syntheses, there is an immediate color change, followed by gradual equilibration over 30 minutes. The supernatant is removed by centrifugation, the precipitate is washed with millipore water to remove any remaining NaCl, and centrifuged again. This is repeated for a total of three washings. Finally, the supernatant is discarded and the precipitate is dried in air at room temperature.

After drying the sample in air, the samples were redispersed into ethanol under sonication for 30 minutes, followed by deposition onto a carbon film TEM grid as shown in Figure 1. The particle sizes were estimated from TEM by manually measuring the lattice fringe diameters of $\sim$100 particles. Additionally, the particles synthesized using less hydrogen peroxide were more readily broken up upon redispersion into ethanol under sonication, suggesting that the hydrogen peroxide either chemically modifies the surface of the particles to make them less hydrophilic,

or causes the formation of harder agglomerations than particles synthesized with less hydrogen peroxide.

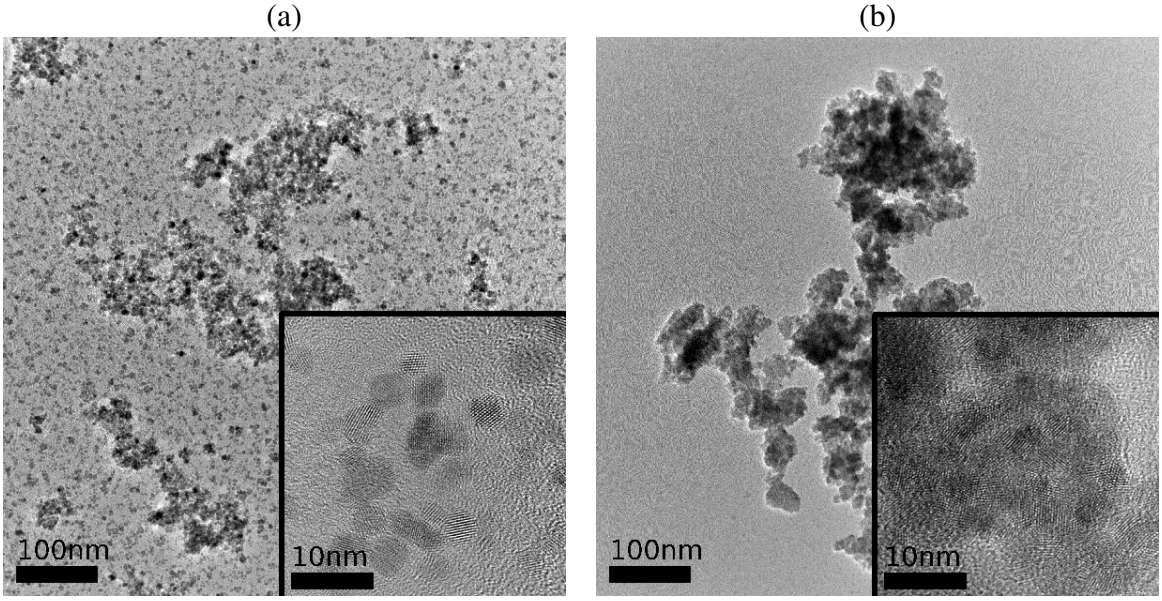

Figure 1: High Resolution TEM of nanocrystalline CeO_2 formed with (a) 0.058:1 H_2O_2:$CeCl_3$ with an average size of 6.2$\pm$1.5 nm and (b) 58:1 H_2O_2:$CeCl_3$ with an average size of 2.3$\pm$0.6 nm. Grids were prepared by redissolving dried powder in ethanol under sonication followed by deposition onto a carbon grid.

The particles were also characterized using a PANalytical X'Pert PRO X-ray Diffractometer (XRD) and peak broadening was used to determine the nanocrystallite size as shown in Figure 2a. The measurements made using TEM were compared to the measurements made using XRD and were shown to be in good agreement as shown in Figure 2b. In cases where larger particles were desired for oxygen vacancy concentration experiments, particles were heat treated to grow to larger sizes.

Oxygen vacancy concentration

X-ray Photoelectron Spectroscopy (XPS) was done on each of the samples in order to determine the approximate oxygen vacancy concentration. In ceria, each oxygen vacancy produces two atoms in the Ce^{3+} oxidation state instead of the typical Ce^{4+} oxidation state. Thus, by measuring the relative

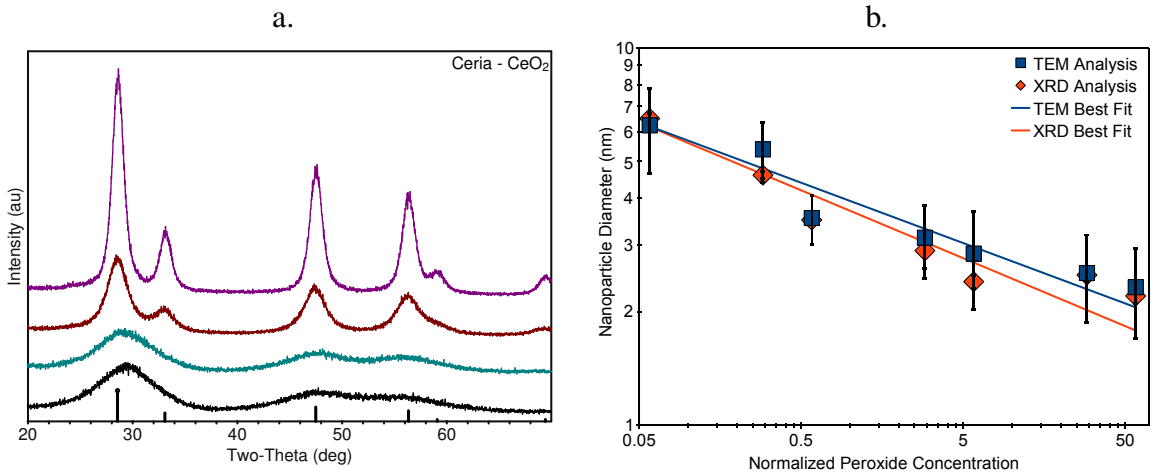

Figure 2: (a) Characteristic XRD spectra showing 0.058:1, 0.58:1, 5.8:1, and 58:1 H_2O_2:$CeCl_3$ during synthesis from top to bottom. (b) Sizes measured with TEM and with XRD compared and shown to have good agreement. At small crystallite sizes, the results diverge both because of the increasing inaccuracy of peak broadening to describe the ensemble size, as well as the increasing difficulty of imaging lattice fringes at small crystallite sizes.

fractions of Ce^{3+} and Ce^{4+}, it is possible to indirectly measure the oxygen vacancy concentration in the material.[10,11,22–27]

Typically, this analysis is done by fitting a model of 10 peaks to the Ce 3d XPS peaks, 6 of which are associated with Ce^{4+} and 4 of which are associated with Ce^{3+}.[10,11,22–25,27] However, we found this analysis to be difficult to do repeatably, with the initial positions and shapes of the peaks dramatically effecting the corresponding oxygen vacancy concentration measured, regardless of the extent to which we constrained the positions of the peaks.

To alleviate this problem, we used principle component analysis (PCA) to reduce the number of independent variables to be optimized from 30 to 2 using the techniques outlined by Holgado *et al.*[26] Using the principle components provided to us by Holgado, a reasonable and repeatable estimate of the oxygen vacancy concentration was achievable (Figure 3). The results of this analysis are shown in Figure 3 as a function of nanoparticle size, showing a trend towards increased oxygen vacancy concentration as particle size decreases.

The functional form of the trend is difficult to determine from this data, but it is known that the oxygen vacancy concentration asymptotes to ~ 0 in the bulk phase. Thus, fitting a simple

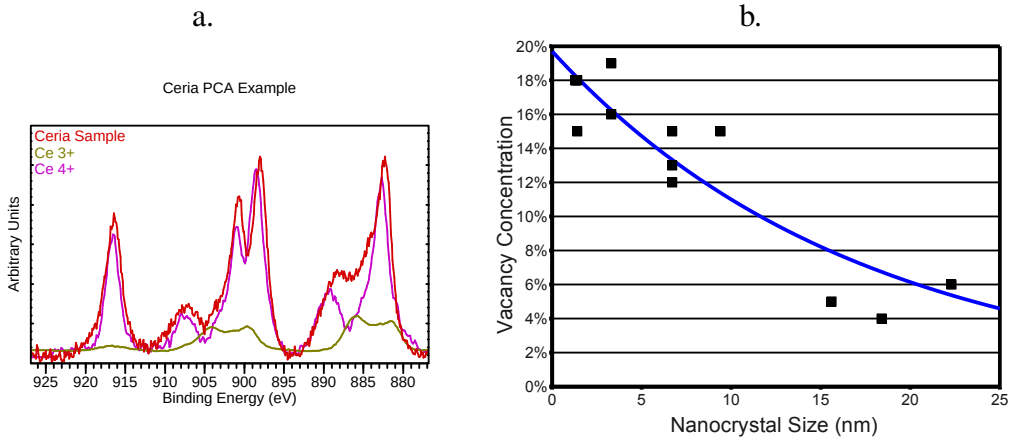

Figure 3: (a) Characteristic XPS spectra, as well as the fitted Ce^{3+} and Ce^{4+} principle components from which the oxygen concentration in the sample is derived. (b) Oxygen vacancy concentrations as a function of nanoparticle size, showing the expected trend of increased vacancy concentration as particle size decreases.

exponential model asympoting to zero gives the form

$$\left[V^{O}\right] = 19.7 \cdot 1.06^{-D} \tag{1}$$

where D is the measured nanoparticle diameter and $\left[V^{O}\right]$ is the oxygen vacancy concentration. However, this fit has a χ^2 of 4.7, so the confidence in this specific relation is poor.

Although XPS is useful only as a relative measure of oxygen vacancy concentration due to the high vacuum necessary and bias towards surface defects, these measurements confirm that the expected trend of increasing oxygen vacancy concentration continues as particle sizes become extremely small, with 1.3 nm particles (as estimated by XRD peak broadening) showing $\sim$18% of all oxygen sites vacant under the high vacuum conditions present during XPS measurements.

To our knowledge, approximations for the functional dependence of oxygen vacancy concentration as a function of nanocrystallite size have only been done previously on limited data sets ($\sim$3-5 measurements), and has only been done on larger particles (3-30 nm), making our measurements valuable as both a more refined dataset as well as for verification that the trend continues down to very small crystallite sizes ($\sim$1.3 nm).[10,11,24]

Sintering Characteristics

The sintering characteristics of 2 nm, 3 nm, and 6 nm nanocrystals were tested by taking periodic XRD spectra of a powder sample pressed into a cup holder and heated to 450°C, 500°C, and 550°C for 2 hours using a PANalytical X'Pert PRO diffractometer with an in-situ furnace. The nanocrystal size was calculated using the full width at half maximum of the isolated ceria {200} peak at 48 degrees. Although using only a single peak reduces the absolute accuracy of an XRD-based size measurement due to the presence of strain in the crystallites, it also allows for time resolution of about 1 min per measurement. This quick measurement time allows for better comparison to time-dependent growth models, especially at early times when particles are growing rapidly. Longer period scans were done before and after the heat treatment to characterize the impact of strain on the particle sizes. Even in the case of 2.0 nm particles where strain went from $\sim$2% to $\sim$0.1%, the change in absolute offset was less than 0.5 nm.

The sintering behavior of powders is not very well understood, so we have applied a simple power-law style growth equation to the system in order to quantify the behavior. We have used the equation

$$D(t)^m - D(0)^m = k \cdot t \tag{2}$$

where $D(t)$ is the average particle diameter as a function of time, m is the "growth exponent", k is the rate constant, and t is the time. This equation is based on a model of diffusion limited coarsening.[28,29]

The rate constant in diffusion-limited systems is frequently modeled as a diffusion rate governed by an Arrhenius type activation energy and prefactor. This can be written as

$$k = C \cdot \exp\left(\frac{-Q}{k_B T}\right) \tag{3}$$

where k is the rate constant in Equation 2, C is a prefactor on the rate characteristic of the sample, Q is an activation energy characteristic of the sample, and T is the temperature. Using this model, it is possible to take time-resolved measurements of the average particle size of a sample at different

temperatures and fit the temperatures simultaneously to this model to calculate the rate constant prefactor, activation energy, and growth rate exponent of the system. With three variables and three sets of temperature data, the system should have a single solution that satisfies an optimal fit to all three temperature data sets.

Each spectrum was analyzed to determine the particle size, and the composite data is shown in Figure 4. Of particular interest is the very high growth exponent, far higher than the growth exponent of approximate three predicted for typical grain growth or diffusion limited growth. Additionally, the particles with the smallest initial size showed a larger difference in growth rate as a function of temperature, as well as a larger overall growth rate at high temperature, than the particles with the largest initial size. The fitted parameters m, Q, and C for these particles are summarized in Table 1.

Table 1: The fitted growth parameters for nanocrystalline CeO_2.

D_0 (nm)	m	Q (eV)	C
6.0	9	1.9	$5{\cdot}10^{26}$
3.1	8	2.8	$4{\cdot}10^{29}$
2.0	8	3.5	$1{\cdot}10^{34}$

Sintering mechanism — Surface defects

As described previously, the size-dependance of the energetics, which does not change as the particles grow, indicates a permanent defect introducted in the initial synthesis stages which is stable at the temperatures investigated. Of the likely defects, oxygen or sodium surface defects were chosen as the mechanism most consistent with the growth behavior. Hydroxide, chloride/oxide-chloride, and nitrogen-based surface defects as well as morphological changes which resists sintering were considered, but ultimately rejected in favor of either sodium or oxygen defects, with oxygen defects seen as the most likely candidate.

First, to determine if low packing density of the powder is causing high resistance to sintering, powders were pressed into a pellet at 39 MPa. These pellets were sintered at 500°C to verify that

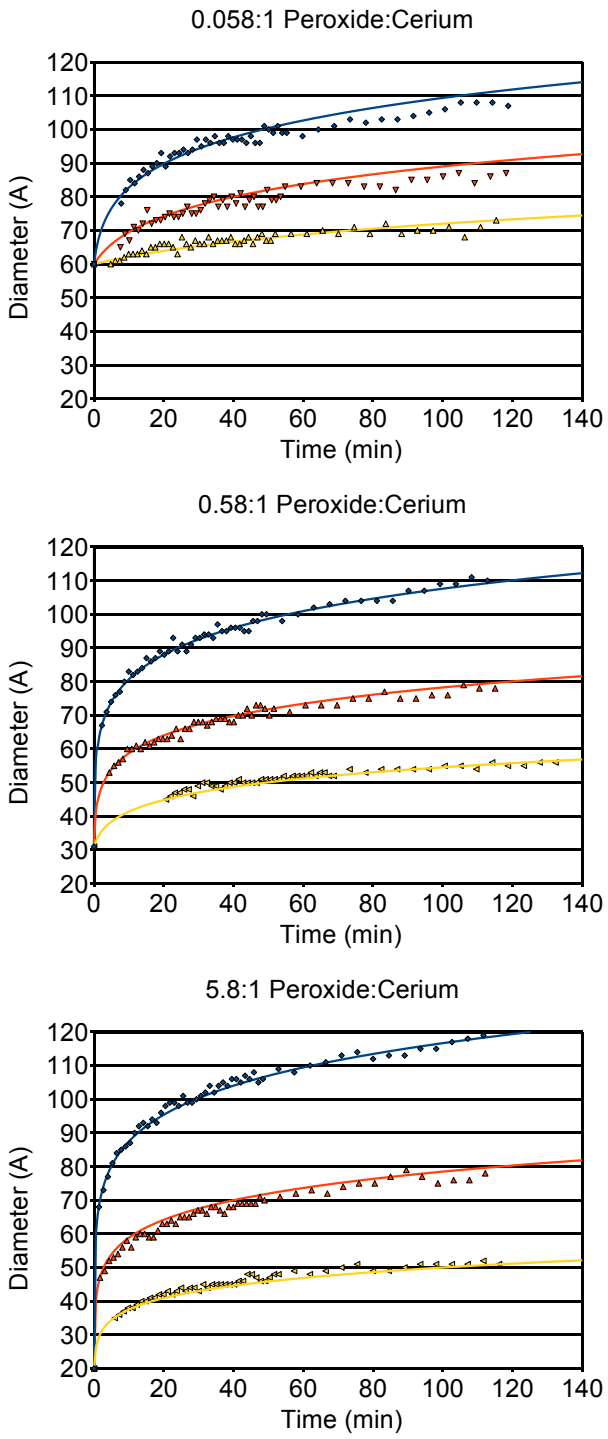

Figure 4: Sintering Behavior of CeO_2 Nanocrystals. (a) 6.0 nm initial size. (b) 3.1 nm initial size. (c) 2.0 nm initial size. Fit lines are plotted based on modeling all three sets of temperature data simultaneously to a power-law model, optimized to minimize total error from the real data by varying activation energy, growth exponent, and prefactor.

the high growth exponent remained, and indeed they showed a growth exponent of $\sim$9, as shown in Figure S1.

Ce-O-Cl defects initially seem to be a likely mechanism as the defects would be stable at high temperature. To investigate this, a comparison synthesis was done using cerium nitrate as a precursor. The resulting sintering profile is shown in Figure S2 alongside a typical chloride synthesis using the same methodology, showing that the two curves are overlapping within the errors of the measurement. The identical sintering shapes suggest that chloride ions are unlikely to be required to produce the observed behavior, either as surface defects, or as residual NaCl. Given the unlikelihood of identical energetics for nitrogen and chlorine based defects, this also most likely rules out nitrogen as a culprit for the sintering resistance. Hydroxide surface defects are also unlikely to survive calcining, as they are generally considered to be very easy to eliminate under heating. However, no direct measurement was done to confirm that hydroxide is not present.

The remaining two surface defect types considered, sodium and oxygen surface defects on the sodium, would be present in samples made from both cerium nitrate and cerium chloride due to the addition of sodium hydroxide. The activation barrier to sintering in the case of very small particles is higher than the barrier for larger particles, so combined with our previous measurement of the oxygen vacancy concentration showing an increase in oxygen vacancy concentration at smaller particle sizes, oxygen seems to be the more likely candidate for the sintering resistance. However, it is difficult to rule out sodium entirely as the increased number of surface cerium atoms could lead to more sodium impurities as well, if they are present at all. Due to the presence of NaCl in the final samples, it was difficult to use XPS to determine whether sodium was present on the surface of the ceria nanocrystals.

There are several mechanisms by which oxygen vacancies could result in heightened thermal stability. First, when the particles begin to combine with their neighbors, a large number of oxygen vacancies would be trapped in the neck, producing pinning points that could act as an energetic barrier to sintering. Second, oxygen defects on the surface of the particles could act as pinning points and lead to a barrier to surface diffusion, likely the dominant transport mechanism at such low

temperatures, and reduce the speed at which particles can merge. Finally, larger particles grown from smaller particles have a lower oxygen vacancy concentration, so the process of sintering the particles also requires the chemical removal of oxygen vacancies, which could represent an energetic barrier to growth based on the distance from the equilibrium oxygen vacancy concentration. It is unclear which of these specific mechanisms is the rate-limiting effect in this system.

Although we were unable to carry out time-resolved sintering tests with steam, the powders were exposed to both air and steam at 400°C for 20 hr and showed significantly greater growth than particles without steam at 400°C, indicating that the presence of steam may eliminate the surface defects causing resistance to sintering. To investigate this possibility, the particles were dried at 120°C directly from the washed precipitate instead of allowing the powder to dry at room temperature before heat treatment. In the case of particles dried at 120° from their water-based paste, the growth was much faster, with a growth expnoent of $\sim$3. Sodium is much less likely to be carried away by steam than oxygen defects, so we conclude that the most likely mechanism for the sintering resistance is the presence of oxygen vacancies on the surface in high concentrations.

Sintering mechanism — Lanthanum doping

Lanthanum was used to coat the nanoparticles and produce an alternative passivation mechanism by mixing lanthanum chloride with cerium chloride during synthesis at 5% and 10% molar ratios. Particles were dried both at room temperature in air as well as at 120°C. The overall growth is shown in Figure 5.

In these tests, the only sample which exhibited low thermal stability was the one dried at 120°C with no La dopant. Even 5% La dopant increases the growth exponent to $m = 7.9$ when dried at 120°C, and 10% La increases the growth exponent all the way to $m = 11.0$. Overall, although the exact numbers for the growth exponent may not be accurate due to differences in the quality of coating, this demonstrates the very high growth exponent caused by surface passivation.

This data provides further evidence that the sintering resistance is not caused by surface chloride or nitride compounds, as the intentionally introduced lanthanum surface defects demonstrate

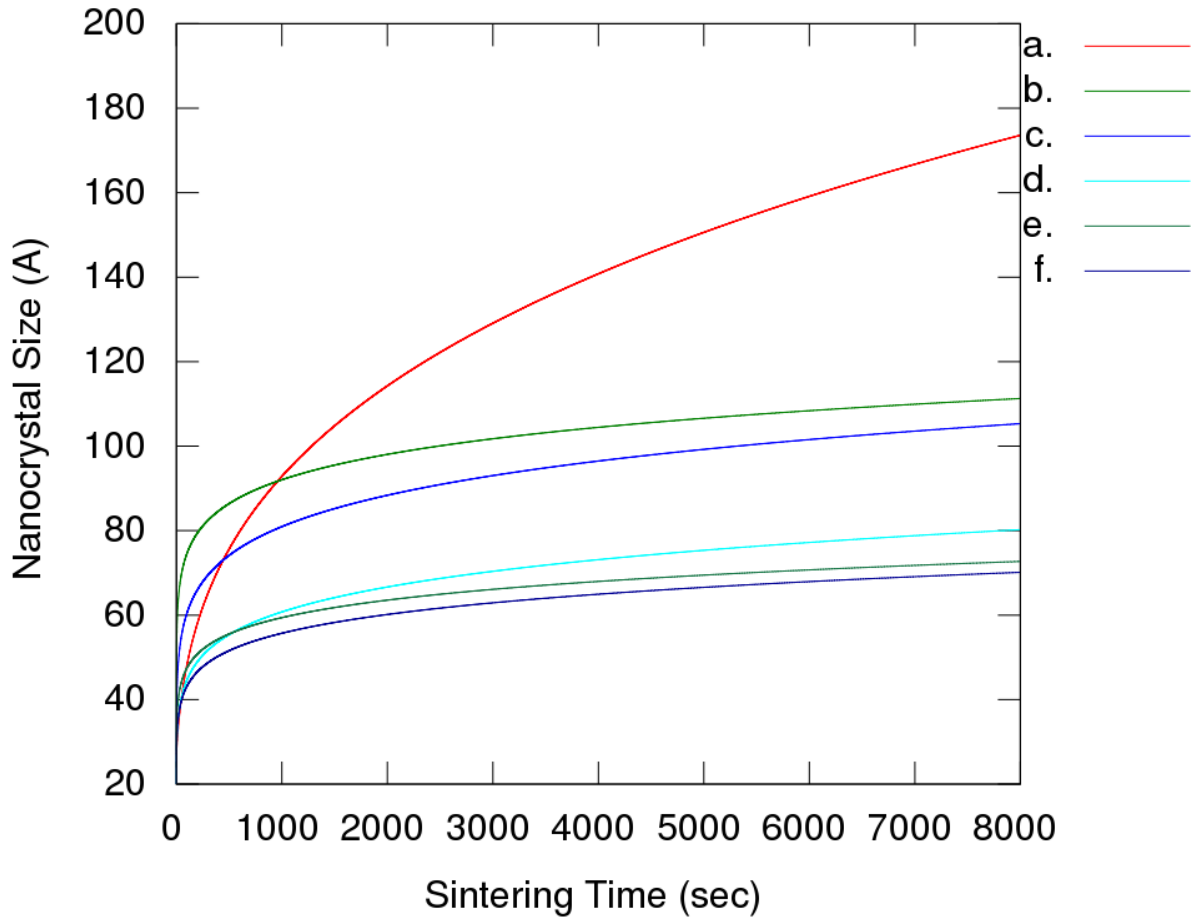

Figure 5: CeO_2 sintering tests done with lanthanum doping. (a) 0% La dried at 120C ($m = 3.3$) (b) 10% La dried at 120C ($m = 11.0$) (c) 5% La dried at 120C ($m = 7.9$) (d) 0% La air dried ($m = 7.5$) (e) 10% La air dried ($m = 10.3$) (f) 5% La air dried ($m = 9.0$)

very different energetics from the as prepared CeO_2 particles using chloride or nitride based precursors. It is also notable that lanthanum-doped ceria particles show further suppressed growth when dried at low temperatures, suggesting a composite effect where both oxygen defects and lanthanum defects are contributing to the sintering resistance.

We have shown in this work a method for performing high-speed ($\sim$1 min) measurements of the sintering behavior of packed nanocrystalline powders of cerium oxide very suitable for use as a catalyst support. By forming extremely small nanocrystals and drying them at room temperature, growth exponents as high as 8-10 can be induced, resulting in significantly greater nanocrystal stability over time. Comparitively, particles dried at higher temperatures (over 120°C) show a growth exponent of only 3. We used a variety of synthetic methods, drying methods, and powder packing methods in order to demonstrate that the most likely mechanism for the increased growth exponent is the presence of oxygen vacancies at high concentrations in the smallest produced nanocrystals ($\sim$1.3 nm). Lanthanum was also incorporated as a dopant into the cerium oxide nanocrystals. These particles were shown to exhibit even further increased resistance to sintering, and the resistance due to surface passivation by lanthanum was not removed by exposure to steam.

We measured indirectly the oxygen defect concentration in 12 nanocrystalline samples of ceria in order to investigate the trends in defect concentration as a function of size, using principle component analysis techniques which proved to be far more repeatable than those typically used in oxygen defect concentration measurements with XPS. Past analyses have only used three or four samples in the size range of 3-30 nm, so this new work represents an unusually large collection of samples measured simultaneously, allowing for a better functional fit. The size of the smallest nanoparticles measured is also smaller than those the authors are aware of in literature, and so are useful for demonstrating the continuation of the existing trends to smaller nanocrystal sizes.

Overall, we recommend the use of lanthanum doped ceria nanocrystals dried at room temperature as the nanocrystals which provide the greatest amount of sintering resistance. Additionally, these very small ceria nanocrystals have an exceptionally high oxygen vacancy concentration, making them potentially very highly advantageous in catalyst applications where nanocrystal growth

is extremely undesirable due to the decreased surface area and oxygen vacancy concentration that growth causes.

Supporting Information Available

XRD-derived sintering data for chloride based cerium oxide pellets, a comparison of sintering data for chloride and nitrate based cerium oxide packed powders, and sintering data comparing various levels and drying methods for lanthanum-doped cerium oxide packed powders.

This material is available free of charge via the Internet at `http://pubs.acs.org`.

Acknowledgement

This work was funded in part by the Army Research Office and the Massachusetts Institute of Technology. The authors thank the MIT Shared Experimental Facilities supported by the MRSEC Program of the National Science Foundation for use of TEM, XPS, and XRD equipment.

We thank Dr. Juan P. Holgado[26] for providing PCA components for Ce^{4+} and Ce^{3+}, without which, analysis of the oxygen defect concentration would have proven very difficult. We also thank Dr. Jeremy Mason and Prof. Chris Schuh at MIT for their consultation with regards to determining the likely mechanisms for growth in this system.

References

(1) Deluga, G. A.; Salge, J. R.; Schmidt, L. D.; Verykios, X. E. *Science* **2004**, *303*, 993.

(2) Kugai, J.; Subramani, V.; Song, C.; Engelhard, M. H.; Chin, Y.-H. *Journal of Catalysis* **2006**, *238*, 430–440.

(3) Kugai, J.; Velu, S.; Song, C. *Catalysis Letters* **2005**, *101*, 255.

(4) Ilieva, L.; Pantaleo, G.; Mintcheva, N.; Ivanov, I.; Venezia, A. M.; Andreeva, D. *Applied Catalysis B: Environmental* **2006**, *65*, 101–109.

(5) Houtman, C. J.; Barteau, M. A. *Journal of Catalysis* **1991**, *130*, 528–546.

(6) *Catalysis by Ceria and Related Materials*; Trovarelli, A., Ed.; Imperial College Press, 2002.

(7) Esch, F.; Fabris, S.; Zhou, L.; Montini, T.; Africh, C.; Fornasiero, P.; Comelli, G.; Rosei, R. *Science* **2005**, *309*, 752.

(8) Fu, Q.; Saltsburg, H.; Flytzani-Stepanopoulos, M. *Science* **2003**, *301*, 935.

(9) Liu, Z.; Jenkins, S.; King, D. *Physical Review Letters* **2005**, *94*, 196102.

(10) Deshpande, S.; Patil, S.; Kuchibhatla, S. V. N. T.; Seal, S. *Applied Physics Letters* **2005**, *87*, 133113.

(11) Zhang, F.; Wang, P.; Koberstein, J.; Khalid, S.; Chan, S. W. *Surface Science* **2004**, *563*, 74–82.

(12) Zerva, C.; Philippopoulos, C. J. *Applied Catalysis B: Environmental* **2006**, *67*, 105–112.

(13) Kuo, L.; Shen, P. *Materials Science and Engineering* **2000**, *A*, 258–265.

(14) Hirta, Y.; Harada, A.; Wang, X. *Ceramics International* **2005**, *31*, 1007–1013.

(15) Bueno-López, A.; nez, I. S.-B.; de Lecea, C. S.-M. *Journal of Catalysis* **2006**, *244*, 102–112.

(16) Colón, G.; Navío, J. A.; Monaci, R.; Ferino, I. *Phys. Chem. Chem. Phys.* **2000**, *2*, 4453–4459.

(17) Djuričić, B.; Pickering, S. *Journal of the European Ceramic Society* **1999**, *19*, 1925–1934.

(18) Scholes, F. H.; Hughes, A. E.; Hardin, S. G.; Lynch, P.; Miller, P. R. *Chem. Mater.* **2007**, *19*, 2321–2328.

(19) Lee, J.-S.; Choi, S.-C. *Materials Letters* **2004**, *58*, 390–393.

(20) Scholes, F. H.; Soste, C.; Hughes, A. E.; Hardin, S. G.; Curtis, P. R. *Applied Surface Science* **2006**, *253*, 1770–1780.

(21) Yamashita, M.; Kameyama, K.; Yabe, S.; Yoshida, S.; Fujishiro, Y.; Kawai, T.; Sato, T. *Journal of Materials Science* **2001**, *37*, 683–687.

(22) Mullins, D. R.; Overbury, S. H.; Huntley, D. R. *Surface Science* **1998**, *409*, 307–319.

(23) Romeo, M.; Bak, K.; Fallah, J. E.; Lenormand, F.; Hilaire, L. *Surface and Interface Analysis* **1992**, *20*, 508–512.

(24) Dutta, P.; Pal, S.; Seehra, M. S.; Shi, Y.; Eyring, E. M.; Ernst, R. D. *American Chemical Society* **2006**, *18*, 5144–5146.

(25) Bodke, A. S.; Bharadwaj, S. S.; Schmidt, L. D. *Journal of Catalysis* **1998**, *179*, 138–149.

(26) Holgado, J.; Alvarez, R.; Munuera, G. *Applied Surface Science* **2000**, *161*, 301–315.

(27) Trudeau, M.; Tschöpe, A.; Ying, J. *Surface and Interface Analysis* **1995**, *23*, 219–226.

(28) Ratke, L.; Voorhees, P. W. *Growth and coarsening: Ostwald ripening in material processing.*; Springer, 2002.

(29) Balluffi, R.; Allen, S.; Carter, C. *Kinetics of Materials*; John Wiley & Sons, 2005.

Graphical TOC Entry

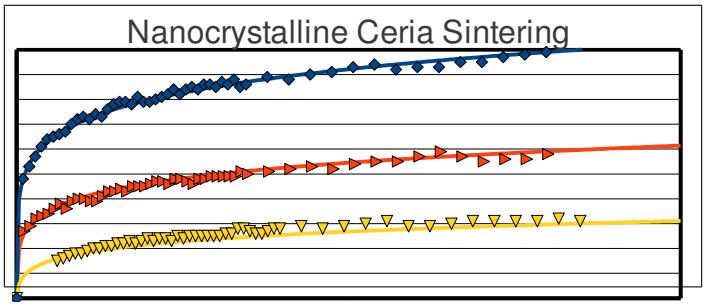

Supporting Information

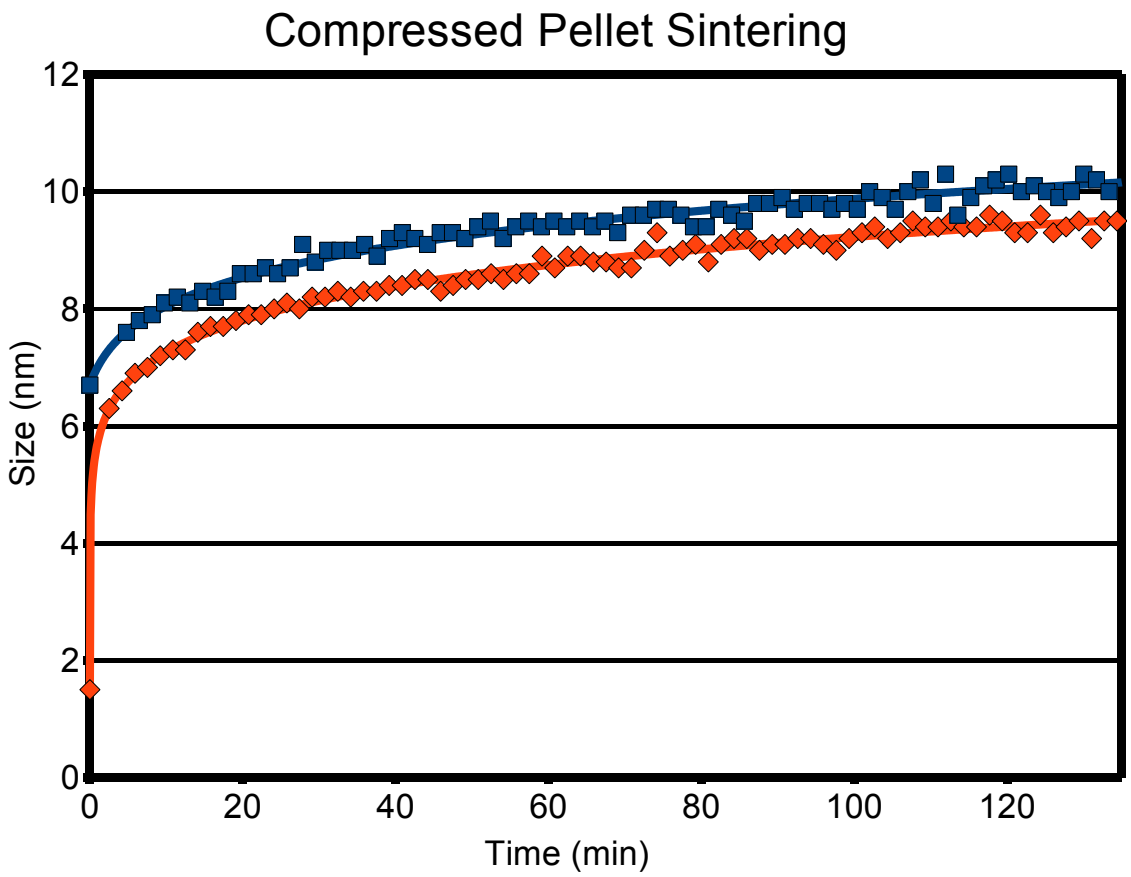

Figure S1: Sintering tests carried out at 500°C for 2 hr to determine if increased packing density eliminates the heightened sintering resistance seen in the powder samples. In the case of both ∼6 nm and ∼2 nm initial nanocrystallite sizes, the growth exponent was ∼9, and in both cases, at equal sizes, the smaller initial particle shows a smaller instantaneous growth rate, consistent with the behavior seen for the powders not pressed into a hard pellet.

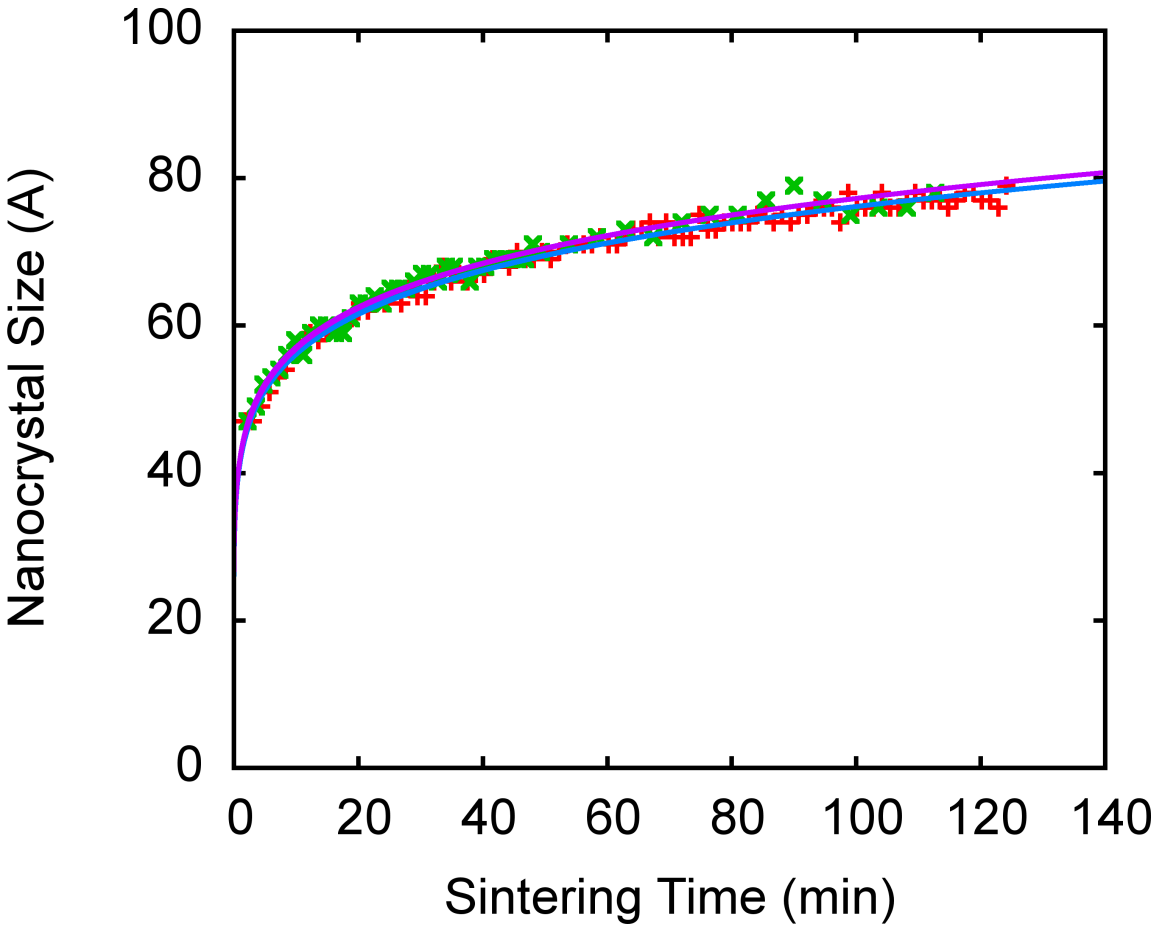

Figure S2: CeO_2 sintering tests done using a nitrate precursor, compared to using a chloride precursor. Both samples were dried at room temperature and done at the same concentrations, and began with identical particle sizes. Both samples exhibit nearly identical growth exponents of $\sim$8.